How far does a fold go?

Atul Bhaskar[a,*], Kevin Jose[a]

[a]*Faculty of Engineering and Physical Sciences,*
Southampton Innovation Boldrewood Campus,
University of Southampton,Southampton,
SO16 7QF, UK

Abstract

We assess the spatial spread of a fold within a narrow elastic strip theoretically and computationally in the small deflection regime. We consider a hierarchy of folding-response ansatz, suitable for stretch-free deformation. The role of Poisson's coupling between the two curvatures, and that of surface twist, is brought out. Here we show that there exists a critical Poisson's ratio separating the regime of monotonically decaying fold profiles from that of decaying oscillatory folds. A spatially separable solution results in length-wise localised folds, the length scale of which is in excellent agreement with that obtained from simulations. The persistence length shows significant sensitivity to the Poisson's ratio of the material. We also establish a mathematical analogy of the folding problem, with one of elastic structures on foundations, the restoring force being proportional to local deflection as well as shear in the foundation.

Keywords: Soft elastic sheets, folds, persistence, Poisson effect

1. Introduction

Folding and bending of soft sheets, filaments and ribbons are of great current interest in biology [1, 2], micro-electronics [3], aerospace skin-structures [4], nano-mechanics of 2D materials such as graphene [5, 6, 7], and stretchable electronics [8]. Thermal fluctuations alone can bend extremely thin films and filaments appreciably. For rods, the spatial decay of response is characterised by the persistence length, which is the ratio of the bending stiffness and the Boltzmann scale factor of energy $k_B T$ (see, e.g. [9]). Decaying elastic response, away from the point of loading, is also associated with Saint-Venant's principle [10], which states that the effect of distribution of loading quickly "dissipates" away from the region of its application, a consequence of which is that a self-equilibrating system of forces must result in a decaying near-field i.e. a vanishing far-field. Spatial decay of response has been estimated for a host of molecular and nano-structures, e.g. long polymer chains [11, 12], DNA and RNA [13, 14], conformations of developable ribbons [15], etc. The role of membrane and bending forces in wrinkling [16] and its suppression [17] as well as its spatial localisation have been reported. Wrinkling has been proposed to measure the modulus of elasticity [18]; the present work suggests the potential of using the persistence of cantilevered films for the metrology of Poisson's ratio. Inspired by practical applications, elastic strips under various loads have been analysed before [19, 20, 21, 22]. However, characterising the spatial localisation of a fold at the edge of an elastic strip has not been
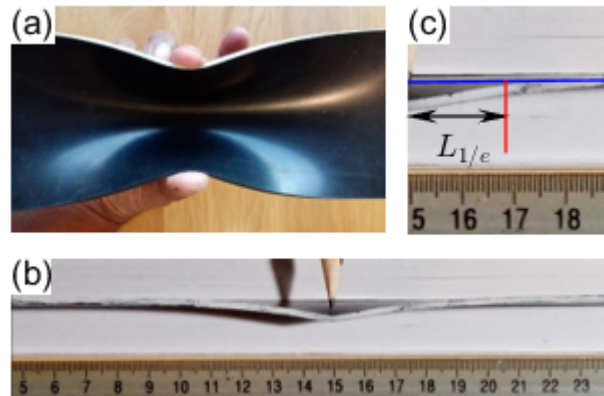

Figure 1: (a) A localised fold on a 2 mm thick soft rubber strip, (b) Edge view of a cantilevered strip poked at a point, (c) Half of the strip in (b) showing a decay length scale $\approx 0.93 \times$ width.

the motivation in these, which is our primary interest here. We will use the word *persistence* in the spirit of [23, 24], who studied a diametrically pinched elastic cylinder.

We define a decay length $L_{1/e}$ as the distance at which the amplitude of the edge profile diminishes to $1/e$ of its value. For a rubber strip (Figure 1(a)), it is estimated as $\approx 1.2 \times b$, where b is the width. The bent profile is deep in the plane perpendicular to that of the paper, which could induce significant non-linearity. A 20 mm wide *cantilevered* strip (Figure 1(b)), poked to a moderate amplitude by a sharp tip (tip displacement $\approx 3 \times t$; t is the thickness) , gives $L_{1/e} \approx 0.93 \times b$ (Figure 1(c)). Consider a toy problem, which consists of a narrow elastic strip of width b, fixed along the long edge $y = 0$ and free at $y = b$.

---

*Corresponding author. E-mail address: a.bhaskar@soton.ac.uk

It is folded at $x = 0$ with a *prescribed* width-wise curvature κ_0. Our primary interest here is in the spatial evolution of the curvature along the length, rather than the response of a poked sheet to a force, when rotations of the normal are small. We ignore membrane energies due to (i) stretch that accompanies bending[1], and (ii) geometric nonlinearity[2]. In the competition to establish equilibrium, their relative importance vis-a-vis bending energy depends on the regime of deflection and the geometric parameters. A simple yet fundamental understanding of the fold relaxation arising from the competition between energies associated with curvatures in the two direction, coupling mediated by Poisson's effect, and the twist energy, appears to be missing. Indeed, here we show that Poisson coupling plays a central role in the persistence of a fold and the simple linear analysis is adequate to produce even the finest details of the curved fold profile, when membrane strains are small.

While we favour simplest mathematical apparatus, beam-like 1D energy expressions are inadequate as staring point, because of the truly 2D nature of surface structures. The strain energy of a bent sheet is associated with two curvatures, Poisson coupling between them, and twist:

$$U = \frac{D}{2} \iint_A \left(w_{xx}^2 + w_{yy}^2 + 2\nu w_{xx} w_{yy} + 2(1-\nu) w_{xy}^2 \right) \mathrm{d}A, \tag{1}$$

where $w(x, y)$ is the transverse deflection of the mid-surface of the sheet originally in the x-y plane, D is the bending stiffness; subscripts denote differentiation. A fold is characterised by curvature, so we consider the spatial evolution of curvature $\kappa(x)$ in the x-direction. The sheet is bent at the origin in the form $w(0, y) = (\kappa_0/2)y^2$. Besides simplicity, inherent to this form is y-wise constancy of curvature. Application of the principle of minimum potential energy, using Equation 1, results in the well known biharmonic partial differential equation and the natural boundary conditions. Attempting to solve the field equation directly, either exactly or approximately, obscures the primary interest here, which is characterising the localisation of a fold. The algebraic difficulty is particularly severe with the free-edge, since the variationally consistent boundary conditions are mathematically arduous, if not intractable.

Here we explore the persistence behaviour of the fold using a hierarchy of simplifications. Throughout our analyses, we assume that the shape of the fold is preserved along x —the direction of *propagation*—as if the shape were modulated along the long edge. This, in effect, turns the problem into a one-dimensional one. Note the use of

---

[1] Due to Gauss' *Theorema Egregium*, a surface cannot bend without stretching or tearing, if its Gaussian curvature changes, Membrane strains (of which, $\partial u/\partial x$ and $\partial v/\partial y$ are the linear components) cause geometry-induced stiffening of sheets when they are curved; the effect is significant for large rotations, not considered here

[2] The non-linear component of the von Karman membrane strain, $(1/2)w_x^2$, needs to be accounted for, when the rotation w_x is not small; see e.g. [25]

the word propagation is not in the sense of waves, but a static shape that evolves spatially along x. The function according to which the spatial evolution of a localised fold takes place, is determined here variationally using various *ansatz*. At first, using an naive bending energy expression, all Poisson's coupling and twist energy terms are ignored and an exponential decay is assumed, with a yet to be determined exponent. Next, $w(x, y)$ is assumed to be separable in x and y without assuming the exponential form. The next level of sophistication considers all terms in Equation 1, but the spatial evolution is assumed to be exponential, the exponent being treated as the generalised coordinate of the problem. Finally, a separable solution is sought which assumes the shape of the fold fixed but modulated by *an unknown function*. An interesting upshot of our analysis is that the decay of the folds is monotonous for values of the Poisson's ratio below a critical, above which the decay is qualitatively different as it becomes oscillatory in addition to being decaying. The spatial evolution of curvature is found to be qualitatively and quantitatively consistent with computational results.

2. Theoretical characterisation of spatially localised folds

Returning to the cantilevered strip, an out-of-plane deflection $w(0, y) = w_0(y/b)^2$ is imposed at $x = 0$. Introduce non-dimensional quantities $\bar{w} = w/w_0$, $\bar{x} = x/b$, $\bar{y} = y/b$. A quadratic shape is the simplest polynomial with non-zero curvature $\kappa_0 = 2w_0/b^2$. Due to symmetry, $\bar{w}_x(0, \bar{y}) = 0$, and only half of the folded structure, $\bar{x} \geq 0$, needs to be considered; $(\bullet)' = \mathrm{d}(\bullet)/\mathrm{d}\bar{x}$. Further, $\bar{w}(0, 1) = 1$, and $\bar{w}(\infty, \bar{y}) = 0$. We present a hierarchy of analyses next, starting with the simplest.

(A) A naive analysis of bi-directional folding. Consider twist-free bending of an elastic sheet, ignoring the Poisson coupling between the two curvatures w_{xx} and w_{yy}, i.e. $U \approx (D/2) \iint_A (w_{xx}^2 + w_{yy}^2) \mathrm{d}A$, to be referred to as Model (A) subsequently. Zero twist in the x-y implies $w_{xy} = 0$, so that x and y are the principal curvature directions at all points. Persistence behaviour suggests x-wise exponential fall, i.e. an ansatz of the form $\bar{w}(\bar{x}, \bar{y}) = \exp(\lambda|\bar{x}|)(\bar{y})^2$. Minimizing the potential energy after this substitution while treating λ as a generalised coordinate, i.e. $\partial U/\partial \lambda = 0$, we have, $\lambda^4 - (20/3) = 0$. Only the negative real root is acceptable since other three roots refer to oscillatory or growing solutions —both unphysical. The persistence length can be defined as $L_P = \ell_P \times b$, where $\ell_P = |\lambda^{-1}|$. So, $\ell_P = (20/3)^{-1/4} = 0.62$, which is independent of the Poisson ratio ν. The symmetry condition $f'(0) = 0$ is violated—this is a limitation of the assumed shape.

(B) Naive strain energy: separable ansatz. Substituting another ansatz $\bar{w}(\bar{x}, \bar{y}) = f(\bar{x})\bar{y}^2$—that has an unknown function $f(\bar{x})$—into the approximate expression $U \approx (D/2) \iint_A (w_{xx}^2 + w_{yy}^2) \mathrm{d}A$, and setting $\delta U = 0$, we
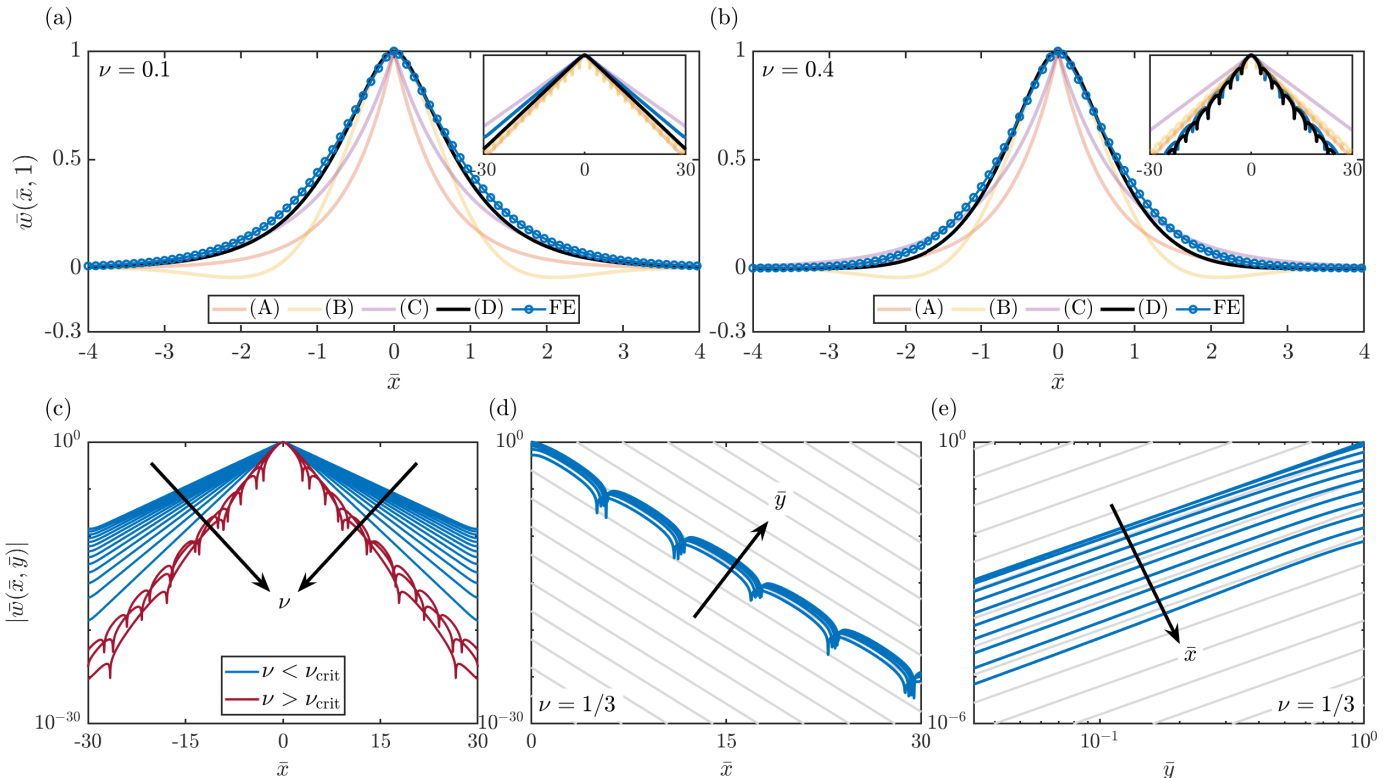
Figure 2: (a) Spatially decaying edge profile predicted by different approaches, for $\nu = 0.1$. (b) Edge profiles for $\nu = 0.4$, showing oscillatory decay. (c) Onset of oscillatory character for $\nu > \nu_{\text{crit}}$ on a semi-log plot. (d) Profiles, $\bar{x} \geq 0$, for each *fixed* $\bar{y}$, show persistence length similar to that predicted analytically. The grey reference lines have slope -1.98 as per analysis (D). (e) The width-wise shape on semi-log plot shows quadratic for each *fixed* $\bar{x}$. The grey reference lines have slope 2.

have $f'''' + 20f = 0$. The characteristic equation is $\lambda^4 + 20 = 0$ with roots $\lambda_{1,2,3,4} = 1.5(\pm 1 \pm i)$. Discarding the spatially growing solutions and imposing $f(0) = 1$ & $f'(0) = 0$, the fold profile is obtained as $\exp(-1.5\bar{x})[\cos(1.5\bar{x}) + \sin(1.5\bar{x})]$; and $\ell_{\text{P}} = 0.67$.

(C) Inclusion of twist & Poisson-coupling. Let us return to the bending energy expression in Equation 1, *retaining all terms*. Like (A), consider an ansatz with x-wise exponential decay, treating λ as a generalised coordinate. Minimising $U(\lambda)$ with respect to λ, we have

$$\lambda^4 + (20/9)(2 - \nu)\lambda^2 - (20/3) = 0. \qquad (2)$$

Note that given the coefficients of the equation we can be sure that the solutions will be of the form $\pm p, \pm qi$ where $p, q > 0$ (supplemental material). Only the negative real root is admissible for finiteness at infinity. An upshot of this is that the decay length scale ℓ_{P} depends on the Poisson's ratio ν. The admissible root is given by

$$\lambda = -\sqrt{\frac{10}{9}\left(-2 + \nu + \sqrt{47/5 - 4\nu + \nu^2}\right)}. \qquad (3)$$

Like (A), the ansatz here violates the symmetry condition $f'(0) = 0$, but all the terms in Equation 1 are now accounted for.

(D) Plate strip folding: separable ansatz. Finally, we seek the *functional form* of the x-dependence of the fold,

within an ansatz of the form $\bar{w}(\bar{x}, \bar{y}) = f(\bar{x})\bar{y}^2$. Substituting this into Equation 1, and variationally minimising U (supplemental material), we obtain

$$f'''' + \gamma f'' + 20f = 0, \qquad (4)$$

where $\gamma(\nu) = (20/3)(3\nu - 2)$. Seeking an exponential solution $\sim \exp(\lambda\bar{x})$, for $\bar{x} > 0$, we obtain the characteristic equation, which is a quadratic in λ^2

$$\lambda^4 + (20/3)(3\nu - 2)\lambda^2 + 20 = 0. \qquad (5)$$

The four roots of Equation 5, depending on the value of ν, are either of the form $\pm p$, $\pm q$ (where $p, q > 0$), or the form $\pm\sqrt{r}\exp(\pm i\theta/2)$, using De Moivre's theorem (where $r, \theta > 0$). In either case, of the four roots there are two with positive real parts associated with spatially growing solutions that must be discarded. The deflected shape can be expressed in terms of the admissible roots (λ_1, λ_2) having negative real part as $f(\bar{x}) = C_1 \exp(\lambda_1\bar{x}) + C_2 \exp(\lambda_2\bar{x})$, where C_1 and C_2 can be determined by imposing the boundary conditions $f(0) = 1$ and the symmetry condition $f'(0) = 0$, so that

$$\bar{w}(\bar{x}, \bar{y}) = \left[\frac{\lambda_2 e^{\lambda_1\bar{x}} - \lambda_1 e^{\lambda_2\bar{x}}}{\lambda_2 - \lambda_1}\right]\bar{y}^2, \qquad (6)$$

for positive $\bar{x}$. When λ_1 & λ_2 are real, the above expression contains *two* decay length scales $|\lambda_1|^{-1}$ and $|\lambda_2|^{-1}$.

3

The larger magnitude root is associated with a faster spatial decay, so it is reasonable that the length over which the fold persists is given by reciprocal of the root with smaller magnitude, i.e. $\ell_P \approx \max(|\lambda_1|^{-1}, |\lambda_2|^{-1})$, which is a function of the Poisson's ratio ν.

When the roots are complex conjugate pair, say $\lambda_{1,2} = (-\rho \pm ik)$, where $\rho > 0$, then the solution has the form $\bar{w}(\bar{x}, \bar{y}) = \exp(-\rho\bar{x})\left[C_1 \sin(k\bar{x}) + C_2 \cos(k\bar{x})\right] \bar{y}^2$. The two constants are determined as before, so that

$$\bar{w}(\bar{x}, \bar{y}) = e^{-(\rho\bar{x})} \left[\left(\frac{\rho}{k}\right) \sin(k\bar{x}) + \cos(k\bar{x})\right] \bar{y}^2. \quad (7)$$

This fold profile is *non-monotonic* and an *oscillatory decay* is observed. There are two *distinct* length scales $\sim \rho^{-1}$ and $\sim k^{-1}$, the first is associated with persistence, the second with spatial oscillation. The decay length scale $\ell_P = 1/\rho$, which again *depends on the Poisson's ratio*, but is *independent* of all other geometric and material parameters. So, the fold spreads over a distance that is a *fixed multiple* of the width b, for a given ν, regardless of the thickness or the modulus of elasticity. Unlike the case of a pair of real admissible roots, there is no ambiguity to be resolved now for persistence based on the reciprocal of the exponent. Note that Equation 7 can also be arrived at by substituting $\lambda_{1,2} = (-\rho \pm ik)$ in Equation 6.

While we accept $\ell_P \approx \max(|\lambda_1|^{-1}, |\lambda_2|^{-1})$ for real λ, and $\ell_P = \rho^{-1}$ for $\lambda = -\rho \pm ik$, as above and, as it is customary, there are potentially profound implications on the actual persistence behaviour of profiles that are not described by a single exponential. Two exponentials, or an exponential multiplied by an oscillatory function, could spatially spread very differently from functions that are described by a single exponential. For example, $L_P = b \times |\lambda|^{-1}$ can be very different from $L_{1/e}$, the length at which the amplitude diminished to $1/e$, when a second length scale involved. When $k = \rho$ in Equation 7 (as also in B), the function decreases to $1/e$ of its value at $\ell_{1/e} = 1.24\rho^{-1}$, as opposed to $\ell_P = \rho^{-1}$. Likewise, for $\nu = 0$, from Equation 5, we obtain $\ell_P = 0.76$, whereas from equation Equation 6, $\ell_{1/e} = 1.10$. Such significant differences between ℓ_P and $\ell_{1/e}$ suggest a more nuanced interpretation of persistence length, when an exponential decay is shaped by an oscillatory function or another exponential, and a caution against a unqualified use of the reciprocal of the magnitude of the real part of the exponent. For single exponentials, $\ell_P = \ell_{1/e}$, of course.

3. Simulations, reconciliation with analysis, and discussions

The localisation behaviour of a fold is now examined computationally. Constant curvature profile $\bar{w}(0, \bar{y}) = \bar{y}^2$ was imposed at the length-wise centre of a sufficiently thin and long elastic strip ($t = b/100$, length $= 60 \times b$, to minimise any end effects). Results obtained from finite element (FE) simulations within the commercial code ANSYS (supplemental material) are taken as benchmark; and
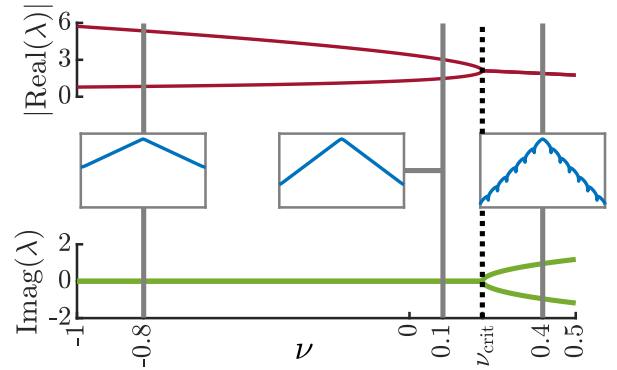

Figure 3: Monotonic-to-oscillatory-decay bifurcation at ν_{crit}. Real and the imaginary parts of λ (analysis D), as functions of ν (top & bottom); fold profiles on a log scale (middle).

those from the four ansatz (A)-(D) are scrutinised against these. Figure 2(a) shows the x-wise profile of the edge as obtained from FE simulations (blue dots, labelled FE), for $\nu = 0.1$. The profile obtained from the naive analysis (A) shows some qualitative semblance with that obtained numerically, except that it under-predicts the decay length. Model (B) produces an x-wise decaying oscillatory profile, which is qualitatively incorrect, since simulations show monotonic decay. Analysis (C) that uses an exponential ansatz in conjunction with strain energy in Equation 1 over-predicts the persistence length. Finally, results from the most sophisticated, yet simple analysis (D), shown in solid black lines, are in excellent qualitative and quantitative agreement with FE simulations. Note that $f'(0) = 0$ is satisfied by profiles obtained from analyses (B) and (D), but not by those from (A) and (C). Figure 2(b) shows corresponding comparisons for $\nu = 0.4$. Insets in both Figure 2(a) and Figure 2(b) show the profile shapes on a log scale —straight lines correspond to monotonic exponential decay, whereas profiles with periodic dips indicate exponentially decaying oscillations. Only analysis (D) captures the detailed shape of the fold profile in the short length scale (main figure) as well as long length scale (insets) consistently. The transition from monotonous decay to an oscillatory one, upon increasing ν, is apparent in Figure 2(c) that shows profiles on a logarithmic scale. One half of the x-wise profiles for different values of $\bar{y}$ are plotted in Figure 2(d) against a background of grey reference lines with a slope -1.98, the real part of $\lambda_{1,2} = -1.98 \pm 0.76i$ obtained from analysis (D). Finally, the family of blue lines in Figure 2(e) are y-wise profiles drawn on a log-log scale for different value of x, which confirms that the curvature does not change significantly along x. The separable ansatz $\bar{w}(\bar{x}, \bar{y}) = f(\bar{x})\bar{y}^2$ is thus justified, as the background lines have a slope 2. The decay length scale $\ell_{1/e} = 0.90$ from model (D) for SBR rubber, $\nu = 0.48$, compares well with the observed value of ≈ 0.93 for the poked cantilevered sheet, and 0.98 obtained numerically.

The relative success of the four approaches in predicting the decay behaviour of a fold is reflected in the values
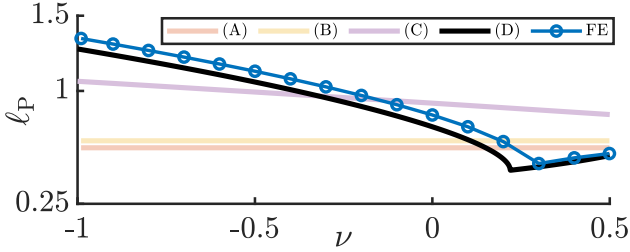
Figure 4: Persistence length as a function of the Poisson's ratio: numerical results vs. analyses. Non-smooth variation is due to transition from monotonic decay to oscillatory decay.

Analytical approach	λ	ℓ_P
Exponential ansatz (naive U): (**A**)	-1.61	0.62
Separable ansatz (naive U): (**B**)	$-1.50 \pm 1.50i$	0.67
Exponential ansatz, U in eq 1: (**C**)	-1.15	0.87
Separable ansatz, U in eq 1: (**D**)	$-1.98 \pm 0.76i$	**0.51**
FE simulation	$-1.90 \pm 0.79i$	**0.53**

Table 1: Decay length scale from various analyses. $\nu = 1/3$.

of λ and ℓ_P tabulated in Figure 3, for $\nu = 1/3$. The exponent obtained by fitting an exponential to $w(x, b)$ from FE matches best with the real part of λ from analysis (D). The decay length scale given by the real part of λ and the length scale of oscillation given by its imaginary part are within 4% of the values obtained from FE. The length scales from FE were ascertained by fitting Equation 6 or Equation 7, depending on value of ν. It can be shown (supplemental material) that the roots of the characteristic equation are complex conjugate for $\nu > \nu_\mathrm{crit}$, where $\nu_\mathrm{crit} \approx 0.22$. Hence the fold has a decaying oscillatory shape for $\nu > \nu_\mathrm{crit}$, whereas it is monotonic for $-1 < \nu < \nu_\mathrm{crit}$. The real and the imaginary parts of λ are plotted against the Poisson's ratio in Figure 3. The transition from a pair to real roots to a pair of complex conjugates retains continuity of the persistence length at the point of bifurcation. The decay behaviour is unremarkable for negative Poisson's ratio—i.e for auxetic materials—as it follows the trend smoothly.

The dependence $\ell_\mathrm{P}(\nu)$ is presented for $-1 < \nu < 0.5$ in Figure 4. Analyses (A) and (B) provide reasonable estimates of persistence around $\nu = 0.1$, but they incorrectly show independence of the characteristic decay length with Poisson's ratio. Model (C) shows predicts monotonic decay of a fold for *all* values of ν, which is incorrect. Again, the simple yet effective model (D) successfully captures all the subtle features of the fold localisation extremely well, as evidenced by the excellent agreement with numerical estimates for ℓ_P.

Having considered two models that include Poisson's coupling between the two curvatures (the second term within the strain energy expression in Equation 1) and twist (the last term in this expression), it is worth asking as to what the inclusion of one and not the other may lead to the persistence behaviour. Without detailed presentation of results, we state that the effect of twist turns out to be significant (supplemental material, figure S4), whereas retaining just the Poisson's coupling term results in an incorrect dependence of the persistence length with respect to the Poisson's ratio for most values of ν. Also, given the use of thin plate theory, thickness is not expected to have an effect on the persistence length. This is confirmed in finite element simulations numerically (explanation and numerical results in figure S3 of supplemental material).

Beam on Pasternak foundation analogy. The spatial decay behaviour of a fold has strong mathematical parallelism with the mechanics of beams on elastic foundations [26] that has had a profound influence on modelling adhesive interactions in soft matter [27]. The simplest elastic foundation model, attributed to Winkler [28], has restoring force proportional to the local deflection. The naive expression of the strain energy of a bent sheet in (B) results in the ODE $f'''' + 20f = 0$, which is formally similar to the beam on elastic foundation $Bf'''' + Kf = 0$, where B is the bending stiffness and K is the stiffness per unit length of the *Winkler* foundation. The solution in (B) of the form $\exp(-kx)\cos(kx + \phi)$ is reminiscent of the pinched tube problem [23, 29], the length scale for decay and oscillations being the same and equal to $k^{-1} \approx 1.5b$, which is independent of all material and structural properties for analysis (B). Contrast this with the fold profile in Equation 7, which is characterised by two length scales, one for decay and one for oscillations—both dependent on the Poisson's ratio. Let us turn to equation (4) that contains the f'' term, which is analogous *Pasternak* elastic foundation [30] $Bf'''' + \gamma f'' + Kf = 0$; the second derivative term is associated with the shear deformation in the foundation. A key difference between the behaviour arising from the Winkler foundation model vs the Pasternak model is that in case of the former, the oscillatory decay has wavenumber of oscillations the same as the reciprocal of the persistence length. For Pasternak model, and also Equation 4, these two length scales are different.

Stretch-free folding, invariance of Gaussian curvature, & higher order effects. A deflection profile of the form $w(x, y) = \exp(\lambda x)y^2$ is not stretch free, as it violates $w_{xx}w_{yy} = w_{xy}$ the condition for preserving the Gaussian curvature. Likewise, a profile of the form $w(x, y) = \exp(\lambda x)g(y)$ requires $g_{yy}g = g_y^2$ for stretch-free deformation, which leads to the trivial fold profile of $w(x, y) = 0$. However, numerical experiments confirm (supplemental material) the theoretically inevitable stretch has minimal influence on persistence. This is consistent with the fact the a cantilevered sheet is unconstrained. The relaxation of a fold is primarily a consequence of the competition between curvatures in the two directions and also significantly influenced by the coupling between them, whereas stretch and non-linearity are higher order effects, when the profile displacement is much greater than the thickness. Yet another higher order effect is through-the-thickness shear, which can be neglected if the thickness of the strip is much smaller than its width b.

4. Conclusions

For a narrow elastic strip, cantilevered along a long edge, and folded at the free edge, the bent shape is localised given by a persistence length that depends only on the width of the strip and Poisson's ratio of the material. There exists a critical Poisson's ratio (ν_{crit}), below which the fold profile decays monotonically, and above which with oscillations. We considered a hierarchy of simple models to bring out the persistence behaviour. A naive analysis that ignores Poisson coupling and twist terms within the elastic plate bending energy expression is unable to bring out detailed feature of the persistence behaviour. A separable ansatz of the bent shape, in terms of curvature modulated by an unknown length-wise function, leads to excellent agreement with numerically simulated results. We identified a mathematical analogy with the problem of a pinched beam of Pasternak foundation. The characteristic decay length is slightly under half to one-and-a-half times the width of the strip, depending on the Poisson's ratio. Unlike the response of an elastic structure that is fairly insensitive to Poisson's ratio, this elastic constant has huge implications to the question of spatial spread of a folded sheet, as the decay length scale varies with Poisson's ratio up to a factor of two to three within the practical range. In the small deflection regime, this length scale can be calibrated, and potentially used to measure Poisson's ratio from thin elastic samples—a property usually difficult to measure directly.

References

[1] M. Arnoldi, M. Fritz, E. Bäuerlein, M. Radmacher, E. Sackmann, A. Boulbitch, Bacterial turgor pressure can be measured by atomic force microscopy, Phys. Rev. E 62 (2000) 1034–1044. doi:10.1103/PhysRevE.62.1034.

[2] J. Dervaux, M. Ben Amar, Morphogenesis of growing soft tissues, Phys. Rev. Lett. 101 (2008) 068101. doi:10.1103/PhysRevLett.101.068101.

[3] A. Boisen, S. Dohn, S. S. Keller, S. Schmid, M. Tenje, Cantilever-like micromechanical sensors, Reports on Progress in Physics 74 (3) (2011) 036101.

[4] C. Thill, J. Etches, I. Bond, K. Potter, P. Weaver, Morphing skins, The Aeronautical Journal 112 (1129) (2008) 117–139.

[5] C. Lee, X. Wei, J. W. Kysar, J. Hone, Measurement of the elastic properties and intrinsic strength of monolayer graphene, Science 321 (5887) (2008) 385–388. doi:10.1126/science.1157996.

[6] W. H. Duan, C. M. Wang, Nonlinear bending and stretching of a circular graphene sheet under a central point load, Nanotechnology 20 (7) (2009) 075702. doi:10.1088/0957-4484/20/7/075702.

[7] M. J. Bowick, A. Košmrlj, D. R. Nelson, R. Sknepnek, Non-Hookean statistical mechanics of clamped graphene ribbons, Phys. Rev. B 95 (2017) 104109. doi:10.1103/PhysRevB.95.104109.

[8] J. A. Rogers, T. Someya, Y. Huang, Materials and mechanics for stretchable electronics, Science 327 (5973) (2010) 1603–1607. doi:10.1126/science.1182383.

[9] F. Gittes, B. Mickey, J. Nettleton, J. Howard, Flexural rigidity of microtubules and actin filaments measured from thermal fluctuations in shape., The Journal of Cell Biology 120 (4) (1993) 923–934.

[10] R. V. Mises, On Saint Venant's principle, Bulletin of the American Mathematical Society 51 (8) (1945) 555–562.

[11] J.-L. Barrat, J.-F. Joanny, Persistence length of polyelectrolyte chains, EPL 24 (5) (1993) 333–338. doi:10.1209/0295-5075/24/5/003.

[12] J. Skolnick, M. Fixman, Electrostatic persistence length of a wormlike polyelectrolyte, Macromolecules 10 (5) (1977) 944–948. doi:10.1021/ma60059a011.

[13] C. Storm, P. C. Nelson, Theory of high-force DNA stretching and overstretching, Phys. Rev. E 67 (2003) 051906. doi:10.1103/PhysRevE.67.051906.

[14] J. S. Mitchell, J. Glowacki, A. E. Grandchamp, R. S. Manning, J. H. Maddocks, Sequence-dependent persistence lengths of DNA, Journal of Chemical Theory and Computation 13 (4) (2017) 1539–1555. doi:10.1021/acs.jctc.6b00904.

[15] L. Giomi, L. Mahadevan, Statistical mechanics of developable ribbons, Phys. Rev. Lett. 104 (2010) 238104. doi:10.1103/PhysRevLett.104.238104.

[16] J. D. Paulsen, E. Hohlfeld, H. King, J. Huang, Z. Qiu, T. P. Russell, N. Menon, D. Vella, B. Davidovitch, Curvature-induced stiffness and the spatial variation of wavelength in wrinkled sheets, Proceedings of the National Academy of Sciences 113 (5) (2016) 1144–1149. doi:10.1073/pnas.1521520113.

[17] A. Bonfanti, A. Bhaskar, Elastic stabilization of wrinkles in thin films by auxetic microstructure, Extreme Mechanics Letters 33 (2019) 100556. doi:10.1016/j.eml.2019.100556.

[18] C. M. Stafford, C. Harrison, K. L. Beers, A. Karim, E. J. Amis, M. R. VanLandingham, H.-C. Kim, W. Volksen, R. D. Miller, E. E. Simonyi, A buckling-based metrology for measuring the elastic moduli of polymeric thin films, Nature Materials 3 (8) (2004) 545–550.

[19] C. W. MacGregor, Deflection of a Long Helical Gear Tooth, Mechanical Engineering 57 (1935) 225–227.

[20] D. L. Holl, Cantilever Plate with Concentrated Edge Load, Journal of Applied Mechanics 4 (1937).

[21] R. C. T. Smith, The bending of a semi-infinite strip, Australian Journal of Scientific Research, Series A: Physical Sciences 5 (1952) 227.

[22] T. J. Jaramillo, Deflections and Moments Due to a Concentrated Load on a Cantilever Plate of Infinite Length, Journal of Applied Mechanics 17 (1950) 67–72.

[23] L. Mahadevan, A. Vaziri, M. Das, Persistence of a pinch in a pipe, EPL 77 (4) (2007) 40003. doi:10.1209/0295-5075/77/40003.

[24] D. Matsumoto, T. G. Sano, H. Wada, Pinching an open cylindrical shell: Extended deformation and its persistence, EPL 123 (1) (2018) 14001. doi:10.1209/0295-5075/123/14001.

[25] T. Barois, L. Tadrist, C. Quilliet, Y. Forterre, How a curved elastic strip opens, Phys. Rev. Lett. 113 (2014) 214301. doi:10.1103/PhysRevLett.113.214301.

[26] M. Hetényi, Beams on elastic foundation: theory with applications in the fields of civil and mechanical engineering, University of Michigan, 1946.

[27] D. A. Dillard, B. Mukherjee, P. Karnal, R. C. Batra, J. Frechette, A review of winkler's foundation and its profound influence on adhesion and soft matter applications, Soft Matter 14 (2018) 3669–3683. doi:10.1039/C7SM02062G.

[28] E. Winkler, Die Lehre von der Elasticitaet und Festigkeit: mit besonderer Rücksicht auf ihre Anwendung in der Technik für polytechnische Schulen, Bauakademien, Ingenieue, Maschinenbauer, Architecten, etc, Vol. 1, Dominicus, 1867.

[29] C. R. Calladine, Thin-walled elastic shells analysed by a Rayleigh method, International Journal of Solids and Structures 13 (6) (1977) 515–530.

[30] P. L. Pasternak, On a new method of analysis of an elastic foundation by means of two foundation constants, Gosudarstvennoe Izdatelstvo Literaturi po Stroitelstuve i Arkhitekture, 1954.